Journal of Physics: Condensed Matter

# High-resolution spectroscopy of $YbAl_3(BO_3)_4$ stoichiometric nonlinear laser crystals

To cite this article: M N Popova *et al* 2008 *J. Phys.: Condens. Matter* **20** 455210

J. Phys.: Condens. Matter **20** (2008) 455210 (6pp) doi:10.1088/0953-8984/20/45/455210

# High-resolution spectroscopy of $YbAl_3(BO_3)_4$ stoichiometric nonlinear laser crystals

**M N Popova[1], K N Boldyrev[1], P O Petit[2], B Viana[2] and L N Bezmaternykh[3]**

[1] Institute of Spectroscopy, Russian Academy of Sciences, 5 Fizicheskaya street, Troitsk, Moscow region 142190, Russia
[2] Laboratoire de Chimie de la Matière Condensée de Paris, CNRS–UMR 7574, Ecole Nationale Supérieure de Chimie de Paris 11, rue Pierre et Marie Curie F-75005 Paris, France
[3] Kirenskii Institute of Physics, Siberian Branch of RAS, Krasnoyarsk 660036, Russia

E-mail: k.boldyrev@mtu-net.ru

Received 11 July 2008, in final form 18 September 2008
Published 13 October 2008
Online at stacks.iop.org/JPhysCM/20/455210

**Abstract**

We present temperature-dependent high-resolution polarized transmittance spectroscopy as well as luminescence spectroscopy of $YbAl_3(BO_3)_4$ single crystals. Positions and symmetries of all the $Yb^{3+}$ crystal-field electronic levels have been found from the analysis of the spectra. Near the main line of the optical transition $^2F_{7/2}(0) \rightarrow {}^2F_{5/2}(0)$ we observe a lot of narrow weak lines. These lines point to the presence of several different distorted sites of $Yb^{3+}$. We analyze the possible origin of the distorted sites. Vibronic structure in transmittance and luminescence spectra was observed and compared with room-temperature Raman spectra.

(Some figures in this article are in colour only in the electronic version)

## 1. Introduction

At the present time, much attention is being given to ytterbium-doped nonlinear crystals for laser applications. $Yb^{3+}$ ions demonstrate several advantages over other rare-earth (RE) ions used in solid-state lasers. In the energy region up to 50 000 $cm^{-1}$, they have only two energy levels, the $^2F_{7/2}$ ground state and the long-living $^2F_{5/2}$ excited state at about 10 000 $cm^{-1}$, which can be efficiently pumped by commercial laser diodes near 980 nm. The quasi-three-level laser with a small difference between the absorption and emission bands can be realized, resulting in a high pump–laser conversion and reduced crystal heating during laser operation. Furthermore, cross-relaxation and excited-state absorption losses are absent.

Another important property of the $Yb^{3+}$ ion is its tendency to couple strongly with matrix lattice vibrations (see, e.g. [1]). This leads to a strong thermal broadening of the electronic transitions and also to the appearance of strong vibronic satellites in the absorption and emission spectra. From the viewpoint of laser applications, a broad spectrum allows the achievement of short laser pulses and also gives the possibility to tune the infrared laser wavelength. The use of a nonlinear crystal as a host matrix for the $Yb^{3+}$ ion extends the wavelength to the visible region through self-frequency doubling (SFD) and self-frequency mixing.

Among nonlinear crystals, $YAl_3(BO_3)_4$ (YAB) possesses not only excellent nonlinear properties but also good mechanical strength, thermal properties and chemical stability. Recently, considerable progress has been achieved in creating compact diode-pumped efficient Yb:YAB lasers. Tunable CW laser action in the near infrared at around 1040 nm [2] as well as in the green (513–546 nm) [3], and yellow (560–570 nm) [4] spectral regions has been demonstrated. The green output power of 1.1 W reported in [3] corresponds to the highest green power achieved by an SFD laser. Also, a pulsed operation of a Yb:YAB laser has been obtained in both the mode-locked [5] and $Q$-switched [6] regimes. Present efforts in the field of Yb:YAB laser crystals are directed, in particular, towards the growth of highly concentrated crystals for microchip lasers. Thus, the growth of Yb:YAB crystals with $Yb^{3+}$ concentrations up to 75 at.% and of the stoichiometric $YbAl_3(BO_3)_4$ (YbAB) crystal has been reported recently [7, 8].

 

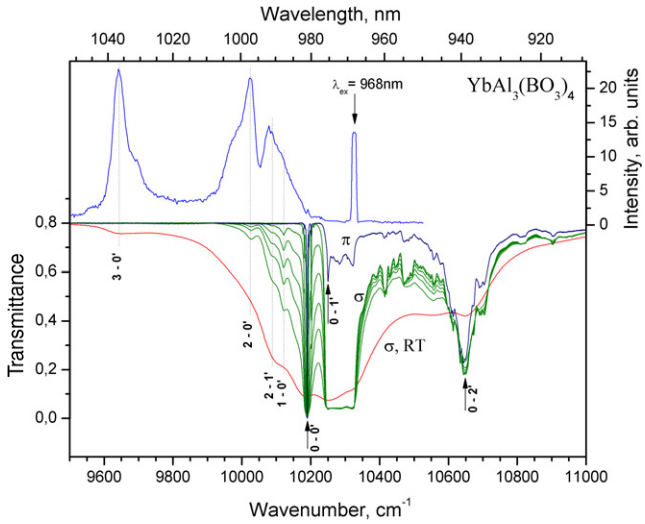


**Figure 1.** Comparison between the LT (20 K) luminescence spectrum of the YbAB crystal under excitation at $\lambda = 968$ nm (upper part) and the $\sigma$ polarized transmittance spectra of the 0.22 mm thick YbAB sample at different temperatures (3.5, 20, 30, 40, 60, 80, and 300 K). The $\pi$ polarized LT (3.5 K) spectrum is also shown.

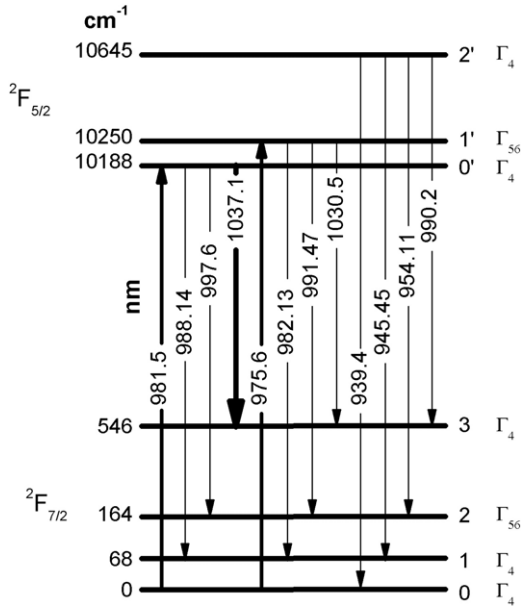


**Figure 2.** Scheme of the energy levels of the $Yb^{3+}$ ion in the YbAB single crystal. The symmetry assignments are indicated on the right.

While a comprehensive spectroscopic study of Yb:YAB crystals with low Yb concentrations (up to 8%) has been performed [9], only room-temperature (RT) spectra of YbAB [8] have been presented up to now. In this paper, we report on the high-resolution polarized temperature-dependent absorption as well as low-temperature (LT) emission spectra of YbAB single crystals. The energies and irreducible representations of the $Yb^{3+}$ levels are determined. Vibronic structure in the spectra is analyzed. The existence of several nonequivalent Yb centers is evidenced. Their quantity does not exceed 1%.

## 2. Experiment

YbAB single crystals of good optical quality were grown by the solution growth technique using the flux 85% mass ($Bi_2Mo_3O_{12} + 2B_2O_3 + 0.5Li_2MoO_4$) + 15%mass $YbAl_3(BO_3)_4$. The crystals were oriented by an optical method and several samples of different thickness were cut either perpendicular or parallel to the $c$-axis of the crystal.

The polarized absorption spectra were measured at 3.5–300 K using a high-resolution Bruker IFS 125 HR Fourier-transform spectrometer with a Si detector and either a closed-cycle Cryomech ST403 cryostat or a helium-vapor cryostat. The resolution for the absorption measurements was up to 0.1 $cm^{-1}$ and was chosen to reproduce correctly the narrowest details in the spectra. The spectra were registered in the $\alpha$ ($k \parallel c$, $E, H \perp c$), $\sigma$ ($k \perp c$, $E, H \perp c$), and $\pi$ ($k \perp c$, $E \parallel c$) polarizations.

In LT luminescence setup, excitation was provided by a CW Ti–sapphire laser (Coherent Innova 90) pumped by an ionized argon laser. The infrared fluorescence was dispersed by an ARC spectrapro 750 monochromator and detected by a liquid-nitrogen-cooled PbS cell. The signal was then amplified by a lock-in amplifier (EG&G) in order to improve the signal-to-noise ratio. Samples were cooled to 10 K with an Oxford Instruments closed-cycle helium cryogenerator. Typical spectral resolution was 0.6 nm in the 1 $\mu$m wavelength region.

In order to measure the ytterbium excited-state lifetime, excitation was provided by an optical parametric oscillator pumped by a pulsed triple Nd:YAG (355 nm). Luminescence was dispersed by an HR 250 Jobin–Yvon monochromator. Finally, the signal was detected by an InGaAs cell in the near-infrared domain.

## 3. Results and discussion

Figure 1 shows the polarized transmittance spectra of about 0.2 mm thick YbAB samples, together with the LT luminescence spectrum. We failed to prepare more thin samples and, at low temperatures, the 0–0′ absorption line (see the scheme of figure 2) is saturated in all the three polarizations ($\pi$, $\sigma$, and $\alpha$), while the region of the next 0–1′ optical transitions is well observed in the $\pi$-polarization but is saturated in the $\sigma$ and $\alpha$-polarized spectra. In the $Yb^{3+}$ free ion, the $^2F_{7/2} \rightarrow {}^2F_{5/2}$ optical transition is allowed in the magnetic dipole approximation. Because of that, one can await a significant magnetic dipole contribution for the $Yb^{3+}$ spectra in the crystal.

In the YbAB crystal that belongs to the trigonal system with the space group R32, $Yb^{3+}$ ions residing in a single crystallographic position experience the crystal field of the $D_3$ point symmetry [10]. This crystal field splits the ground and excited level into four and, respectively, three Kramer's doublets, namely, $^2F_{7/2} \rightarrow {}^3\Gamma_4 + \Gamma_{56}$, $^2F_{5/2} \rightarrow {}^2\Gamma_4 + \Gamma_{56}$ (here, $\Gamma_4$ and $\Gamma_{56}$ are different irreducible representations of the $D_3$ point group). Selection rules for both electric dipole and magnetic dipole optical transitions are summarized in

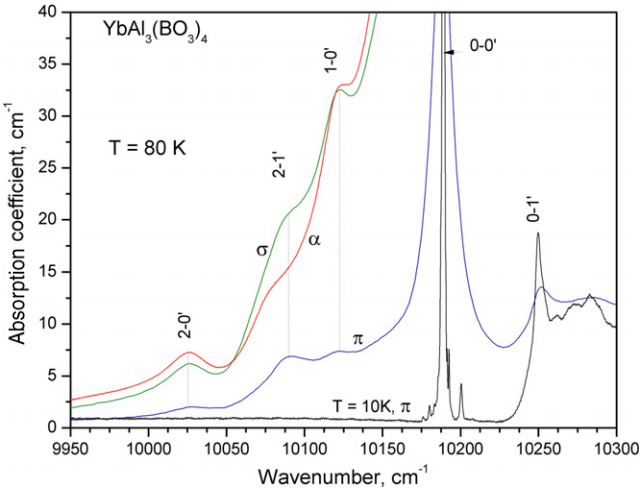


**Figure 3.** A part of the LT spectra of YbAB at $T = 80$ K ($\alpha$, $\pi$, and $\sigma$ polarizations) and at 10 K ($\pi$-polarization).

**Table 1.** Selection rules for electric (d or el) and magnetic ($\mu$ or m) optical transitions in the $D_3$ point symmetry.

| | $\Gamma_4$ | $\Gamma_{56}$ |
|---|---|---|
| $\Gamma_4$ | $d_z\mu_z d_{xy}\mu_{xy}$<br>$(\alpha,\pi,\sigma)_{el}$, $(\alpha,\pi,\sigma)_m$ | $d_{xy}\mu_{xy}$<br>$(\alpha,\sigma)_{el}$, $(\alpha,\pi)_m$ |
| $\Gamma_{56}$ | $d_{xy}\mu_{xy}$<br>$(\alpha,\sigma)_{el}$, $(\alpha,\pi)_m$ | $d_z\mu_z$<br>$(\pi)_{el}(\sigma)_m$,<br>$\alpha$-forbidden |

table 1. The notation of the type $(\alpha,\sigma)_{el}$, $(\alpha,\pi)_m$ indicates that the transition is allowed in the $\alpha$ and $\sigma$ polarizations for the electric dipole case and in the $\alpha$ and $\pi$ polarizations for the magnetic dipole case. The equality $\alpha = \sigma$ points to a purely electric dipole transition while $\alpha = \pi$ holds for a purely magnetic dipole transition. If both electric and magnetic dipoles contribute, it is not possible to distinguish between $\Gamma_4 \rightarrow \Gamma_4$ and $\Gamma_4 \rightarrow \Gamma_{56}$ transitions by inspection of polarized spectra. On the contrary, $\Gamma_{56} \rightarrow \Gamma_{56}$ transitions are strictly forbidden in the $\alpha$-polarization. From the fact that no absorption line vanishes at low temperature in the $\alpha$-polarization, we conclude that the ground state (0) is the $\Gamma_4$ state.

At elevated temperatures, the excited crystal-field (CF) levels of the $^2F_{7/2}$ ground manifolds are populated and give rise to the absorption lines at the low-frequency side from the 0–0′ line. One can see these lines in figure 1 for the $\sigma$-polarized spectrum at different temperatures. Figure 3 displays this spectral region for the $\pi$, $\sigma$, and $\alpha$ polarized spectra of YbAB at $T = 80$ K. The absence of the 2–1′ absorption line in $\alpha$-polarization is evident (we confirmed this statement by subtracting the $\alpha$-spectrum from the $\sigma$-one). Thus, the levels $^2F_{7/2}$ (2) and $^2F_{5/2}$ (1′) are $\Gamma_{56}$ levels. The main luminescence lines correspond well with the excited-state absorption lines (see figure 1). The 0′–0 line is either completely absent in the luminescence spectra or seen as a small bump, which is due to reabsorption of resonant radiation.

The energy levels of YbAB and symmetry assignments are summarized in figure 2. For a comparison, we list the data on

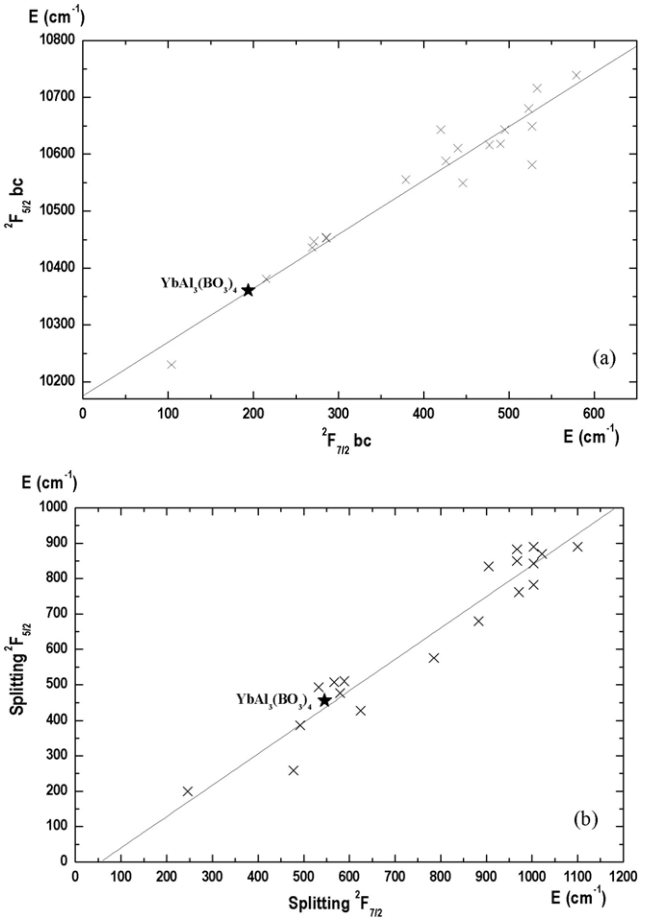


**Figure 4.** The position of YbAB crystal-field levels at the 'barycenter curve' [10] (a) and at the splitting $^4F_{5/2}$ versus $^4F_{7/2}$ curve [11] (b).

$Yb^{3+}$–YAB obtained from the analysis of polarized absorption and of luminescence spectra [9]: 0 ($\Gamma_4$), 77, 165, 565, 10 188 ($\Gamma_4$), 10 248 ($\Gamma_{56}$), 10 660 ($\Gamma_4$). The energy level patterns are similar in both crystals. Figure 4 shows the position of YbAB CF levels at the 'barycenter curve' [11] and the splitting $^4F_{5/2}$ versus $^4F_{7/2}$ curve [12]. It fits this empirical dependence very well, which confirms the reliability of the electronic level positions found from the experimental data.

In several previous works on Yb:YAB, the doublet structure of the 0–0′ absorption and/or 0′–0 emission transition at low temperatures was reported [13, 14, 9]. The relative intensities of two narrow 0–0′ absorption peaks at 10 188 and 10 202 $cm^{-1}$ changed with ytterbium content in the samples, which indicated that these two lines originate from two nonequivalent $Yb^{3+}$ centers in YAB [9]. Correspondingly, the two components of the 0′–0 emission doublet had different excitation spectra. The relative contribution of the minor Yb2 center Yb2/Yb1 was shown to grow from about 3% to 25% with the growth of Yb concentration in the crystal from 0.25% to 8%, respectively [9].

In the LT spectra of YbAB, the satellite line 10 201 $cm^{-1}$ of the 0–0′ absorption transition at 10 189 $cm^{-1}$ is also present (see figure 3). However, several more very narrow lines (with half-widths of several tenth of wavenumber) are observed near the 0–0′ absorption line. Figure 5 shows them in the expanded

**Table 2.** Satellites of the 0–0′ absorption line. Numbers near satellites correspond to notations of figure 5, $\Delta\nu$—distance from the main line, $\delta\nu$—full-width at half-height (FWHH), $S = \int k(\nu)\mathrm{d}\nu$—integral intensity (here $k$ is the absorption coefficient).

| No. | 1 | 2 | 3 | 4 | 5 | 6 | 7 | 8 | 9 | 10 |
|---|---|---|---|---|---|---|---|---|---|---|
| $\Delta\nu$ ($\mathrm{cm}^{-1}$) | 19.3 | −12.5 | 11.7 | −8.6 | −5.4 | 3.9 | −3.1 | 2.7 | 1.9 | 1.3 |
| $\delta\nu$ ($\mathrm{cm}^{-1}$) | 1.08 | 1.00 | 1.59 | 0.97 | 1.06 | 0.64 | 1.13 | 0.38 | 0.36 | 1.13 |
| $S$ ($\mathrm{cm}^{-2}$) | 0.74 | 0.49 | 8.78 | 2.01 | 1.89 | 6.86 | 4.81 | 1.75 | 3.00 | 20.5 |

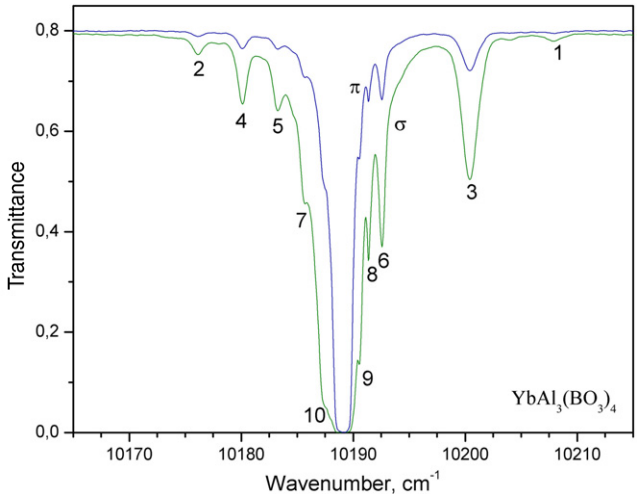


**Figure 5.** Narrow lines near the 0–0′ absorption line of the 0.22 mm thick YbAB single crystal at $T = 3.6$ K.

scale but table 2 lists their parameters. The main absorption 0–0′ line being saturated, it is not possible to determine the relative intensities of the satellite lines. However, from the $\pi$-spectrum of figure 5 we find $k = 4.6\ \mathrm{cm}^{-1}$ for the absorption coefficient in the maximum of the 10 201 $\mathrm{cm}^{-1}$ absorption line, corresponding to the Yb2 center of [9], and get an estimate $k > 330\ \mathrm{cm}^{-1}$ for the saturated main line. This leads to a crude estimate for the relative quantity of Yb2 centers: Yb2/Yb1 < 1.4%.

The discussed satellites, probably, correspond to the $Yb^{3+}$ ions in a regular position but with some defect present in the nearest surrounding. In [15], a very similar satellite structure in the spectra of YAG:$Er^{3+}$, grown by the Czochralski method, has been assigned to the Er centers distorted by nearby defects of the type 'yttrium at the place of aluminum'. Despite a big difference in the ionic radii $r$, $Y^{3+}$ ($r = 0.89$ Å) enters into the position of $Al^{3+}$ ($r = 0.53$ Å) in the course of a high-temperature crystal growth process. In a recent paper [16] a direct comparison between the spectra of $Gd_3Ga_5O_{12}$:$Nd^{3+}$ crystals grown by the Czochralski method and by the solution growth technique at lower temperatures has shown that really in the first case the satellites in the spectra are much stronger. Similar results have been obtained for $YVO_4$:$Nd^{3+}$ grown by Czochralski and solution growth techniques [17]. YbAB crystals are grown by solution growth techniques at lower temperatures, using $K_2Mo_3O_{10}$ and $Bi_2O_3$ flux. Flux ingredients can, however, substitute for a regular ion in the crystal lattice during crystallization. Most probably, $Bi^{3+}$ ($r = 1.02$ Å) substitutes for a rare earth but $Mo^{3+}$ ($r = 0.67$ Å) substitutes for aluminum. Using the structural data on

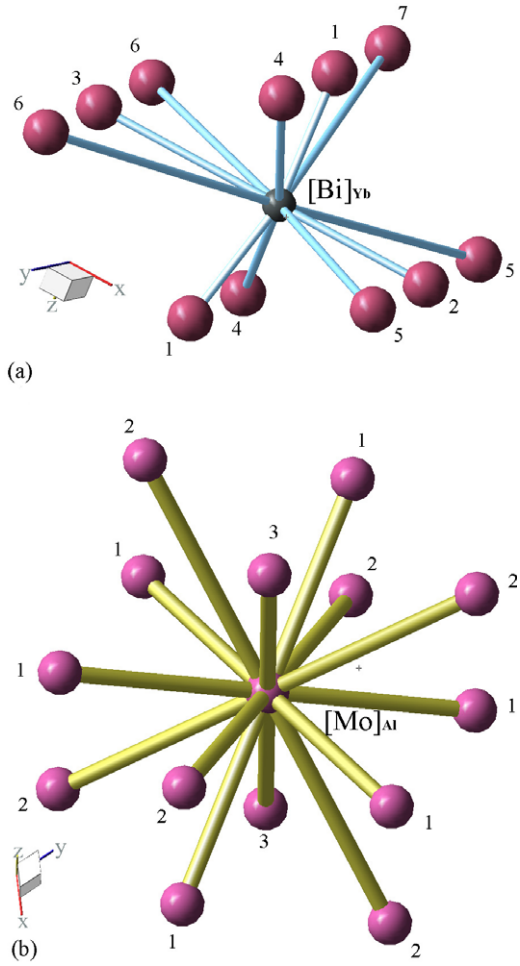


**Figure 6.** Regular $Yb^{3+}$ positions within several coordination spheres of the defects $[Mo]_{Al}$ (a) and $[Bi]_{Yb}$ (b). Numbers near Yb atoms correspond to the coordination sphere numbers (first, second, ...) Yb atoms belong to.

YbAB [18] and the program 'Balls and Sticks' we have found regular $Yb^{3+}$ positions within several coordination spheres of the defects $[Bi]_{Yb}$ and $[Mo]_{Al}$. Figure 6 shows these positions but table 3 lists their distances $R$ from the defect. The shorter $R$ is the stronger is the crystal-field distortion for a given $Yb^{3+}$ ion and the bigger is the spectral displacement of a satellite from the main line, while the intensity should be proportional to the number of equivalent $Yb^{3+}$ centers around a defect. The observed satellite lines have different line widths ranging from 0.4 to 1.3 $\mathrm{cm}^{-1}$, probably because several slightly different distorted Yb positions contribute to a particular satellite line. Table 2 contains the observed distances of satellites from the main line, their widths, and integral intensities. However, it

**Table 3.** Distances between defects ($[Mo]_{Al}$ and $[Bi]_{Yb}$) and several nearest neighbor Yb ions. The number of Yb positions in a given coordination sphere is indicated in parenthesis.

| Coordination sphere no. | 1 | 2 | 3 | 4 | 5 | 6 | 7 |
|---|---|---|---|---|---|---|---|
| $[Mo]_{Al}$–Yb (Å) | 3.619 (2) | 4.153 (1) | 5.098 (1) | 5.507 (2) | 7.178 (2) | 7.763 (2) | 8.026 (1) |
| $[Bi]_{Yb}$–Yb (Å) | 5.854 (6) | 7.176 (6) | 7.189 (2) | | | | |

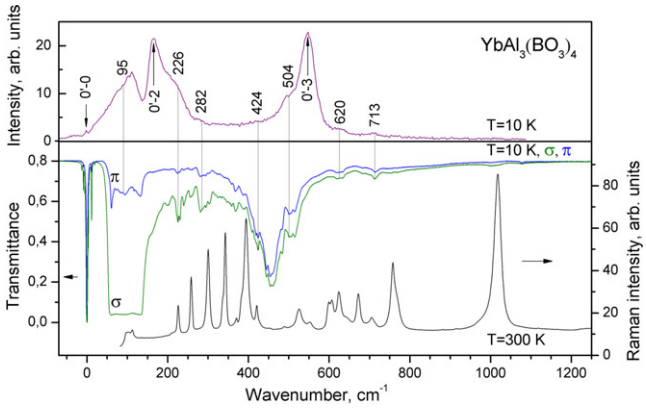


**Figure 7.** Low-temperature emission and transmission spectra plotted symmetrically relative to the 0–0′ transition and compared with the RT Raman spectrum (the lowest curve).

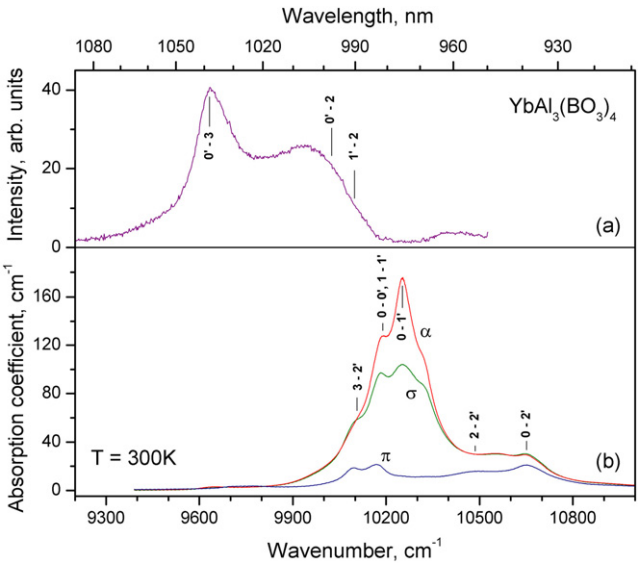


**Figure 8.** The RT emission ($\lambda_{ex} = 940$ nm) (a) and absorption (b) spectra.

is difficult to assign unambiguously a satellite to a particular distorted Yb center, without performing calculations of lattice and crystal-field perturbations by the defect.

In this study, the YbAB crystals were grown using the $Bi_2Mo_3O_{12}$ based flux where $Bi_2O_3$ is strongly bonded to $MoO_3$ which strongly diminishes the probability of the Bi → Yb and Mo → Al substitutions. Possibly because of that, the amount of distorted Yb sites in our crystals was relatively low (<1.4% in contrast to 3–25% reported for Yb:YAB earlier [9]).

As has already been mentioned above, $Yb^{3+}$ ions tend to couple strongly with lattice vibrations. Because of that, vibronic lines appear in the spectra with an intensity comparable to that of electronic lines. Figure 7 shows the absorption and emission spectra plotted symmetrically relative to the 0–0′ transition. Though the luminescence spectrum, being taken at a poor resolution and at effectively higher temperature (due to heating by laser light), does not show such a detailed structure as the absorption spectrum, several coincidences are evident. These spectral details correspond to the vibronics associated with the 0–0′ transition and involve lattice phonons with frequencies 95, 226, 282, 424, 504, 620, and 713 $cm^{-1}$. All these frequencies excluding 95 $cm^{-1}$ (which was outside the studied spectral region) were present in our Raman spectra of YbAB also shown in figure 7. It should be mentioned that the Raman (and the far-infrared spectra) give information on the frequencies of phonons at the Brillouin zone center while the electrons of an RE ion interact with all the phonons. Here, the phonon density of states (multiplied by the electron–phonon interaction constants) is of importance (see, e.g. [19]). A detailed analysis of Raman, far-infrared, and vibronic spectra of YbAB will be presented elsewhere.

For laser applications, the RT spectral properties are important. Figure 8 shows the RT absorption and emission spectra. While the 0–2′ high-frequency absorption band (see figure 8(b)) is equally intense in the $\alpha$ and $\sigma$ polarizations ($\alpha = \sigma$) which points to a purely electric dipole character of the optical transition, in the region of 0–0′ and 0–1′ transitions the $\alpha$-polarized absorption dominates over the $\sigma$-polarized one, evidencing a magnetic dipole contribution to the optical transition probability. The highest absorption coefficient of $k = 175$ $cm^{-1}$ is at the wavelength 975.6 nm (0–1′ transition) in the $\alpha$-polarization. The FWHH of the strong band peaking at 975.6 nm is 200 $cm^{-1}$. Such a broad band is favorable in the case of a possible drift of the pumping diode laser wavelength. The RT lifetime is $\tau = 30$ $\mu$s, which is in agreement with previously reported data [20].

Maximal intensity of the RT luminescence of YbAB corresponds to the 0′–3 transition at ∼1037 nm where the laser action was first obtained for Yb:YAB [2]. A broad emission spectrum could be favorable for some tunability around this wavelength and for producing ultrafast pulse generation in the thin disk configuration.

## 4. Conclusions

Absorption and luminescence spectra of the $YbAl_3(BO_3)_4$ stoichiometric nonlinear crystals were measured in a wide temperature range. The absorption spectra were registered in the $\alpha$ ($k \parallel c$, $E, H \perp c$), $\sigma$ ($k \perp c$, $E, H \perp c$), and $\pi$ ($k \perp c$, $E \parallel c$) polarizations. Positions and symmetries of all the $Yb^{3+}$ crystal-field electronic levels have been found from the analysis of the spectra. In particular, the $\Gamma_{56}$ symmetry of the levels 2 ($^2F_{7/2}$) and 1′ ($^2F_{5/2}$) was established. Multiple weak narrow (down to 0.3 $cm^{-1}$) spectral lines have been found near the $^2F_{7/2}(0) \rightarrow {}^2F_{5/2}(0)$ main line and assigned to $Yb^{3+}$ sites perturbed by a nearby defect. The relative quantity of the perturbed sites was estimated to be less than 1.4%. Vibronic transitions mediated by the electron–phonon coupling were observed and partly assigned.

Finally, the RT optical properties important for laser applications were discussed. At RT, the strongest absorption (characterized by the absorption coefficient $k = 175$ $cm^{-1}$) experiences the $\alpha$-polarized light with the wavelength $\lambda = 975.6$ nm. The width of this absorption band constitutes 200 $cm^{-1}$. It contains both electric dipole and magnetic dipole contributions. The RT fluorescence lifetime was found to be $\tau \sim 30$ $\mu$s.

## Acknowledgments

The authors thank E Antic-Fidancev for helpful discussions on the ‘barycenter curves’, P Aschehoug for technical assistance, and B Mavrin for assistance in Raman spectra measurements. This work was supported by the CNRS–RAS exchange program (project No. 21241), by the Russian Foundation for Basic Research (Grants Nos 07-02-01185 and 06-02-16088), and by the Russian Academy of Sciences under the Programs for Basic Research.

## References

[1] Ellens A, Andres H, ter Heurdt M L H, Wegh R T, Meijerink A and Blasse G 1997 *Phys. Rev.* B **55** 180
[2] Wang P, Dawes J, Dekker P and Piper J 2000 *Opt. Commun.* **174** 467
[3] Jiang H, Li J, Wang J, Hu X-B, Liu H, Teng B, Zhang C-Q, Dekker P and Wang P 2001 *J. Cryst. Growth* **233** 248
[4] Burns P, Dawes J, Dekker P, Piper J, Li J and Wang J 2002 *Opt. Commun.* **207** 315
[5] Lederer M, Hilderbrandt M, Kolev M, Luther-Davies B, Taylor B, Dawes J, Dekker P, Piper J, Tan H and Jagadish C 2002 *Opt. Lett.* **27/6** 436
[6] Dekker P, Dawes J and Piper J 2005 *J. Opt. Soc. Am.* B **22** 378
[7] Liao J, Lin Y, Chen Y, Luo Z and Huang Y 2004 *J. Cryst. Growth* **267** 134
[8] Xu Y, Gong X, Chen Y, Huang M, Luo Z and Huang Y 2003 *J. Cryst. Growth* **252** 241
[9] Ramírez M, Bausá L, Jaque D, Cavalli E, Speghini A and Bettinelli M 2003 *J. Phys.: Condens. Matter* **15** 7789
[10] Mills A D 1960 *Inorg. Chem.* **1** 960
[11] Antic-Fidancev E 2003 What kind of information is possible to obtain from $^{2S+1}$L terms of $4f^N$ configurations? *Physics of Laser Crystals* ed J-C Krupa and N A Kulagin (Dordrecht: Kluwer) pp 75–91
[12] Antic-Fidancev E, Hölsä J and Lastusaari M 2003 *J. Phys.: Condens. Matter* **15** 863
[13] Wang P, Dawes J M, Dekker P, Knowles D S, Piper J A and Lu B 1999 *J. Opt. Soc. Am.* B **16** 63
[14] Földvári I, Beregi E, Baraldi A, Capelletti R, Ryba-Romanowski W, Dominiak-Dzik G, Munoz A and Sosa R 2003 *J. Lumin.* **102/103** 395
[15] Agladze N I, Bagdasarov H S, Vinogradov E A, Zhekov V I, Murina T M, Popova M N and Fedorov E A 1988 *Kristallografiya* **33** 912 (in Russian)
[16] Kaminskiy A A, Butashin A V, Aleksandrov A S, Bezmaternykh B Z, Temerov V L, Gudim I A, Kravtsov N V, Firsov V V, Seo D T, Hommernih U, Templ D and Bro A 2002 *Kristallographiya* **47** 344 (in Russian)
[17] Guillot-Noel O, Viana B, Vivien D, Zogo-Mboulou G B, Jandl S and Moncorgé R 1998 *Ann. Phys. Fr.* **23** 159
[18] Xu Y, Chen Y, Luo Z, Chen J and Huang Y 2002 *Chin. J. Struct. Chem.* **21** 402
[19] Malkin B Z 2005 Ion-phonon interactions *Spectroscopic Properties of Rare Earth Optical Materials* (*Springer Series in Materials Science* vol 83) ed G Liu and B Jacquier (New York: Springer) p 130
[20] Huang Z, Gong X, Huang Y and Luo Z 2004 *Opt. Commun.* **237** 389